Study of bending angle and shadow in a new Schwarzschild-like black hole affected by plasma and non-plasma mediums*

Riasat Ali[1†] Tiecheng Xia[1‡] Muhammad Awais[2§] Rimsha Babar[3¶]

[1]Department of Mathematics, Newtouch Center for Mathematics of Shanghai University, Shanghai 200444, China
[2]Department of Mathematics, University of Engineering and Technology Lahore-54890, Pakistan
[3]Department of Mathematics, GC University Faisalabad Layyah Campus, Layyah-31200, Pakistan

Abstract: In this study, we analyze the models of the deflection angle of a new Schwarzschild-like black hole (BH) and employ the optical metric of the BH. To achieve this, we use the Gaussian curvature of the optical metric and the Gauss-Bonnet theorem, known as the Gibbons-Werner technique, to determine the deflection angle. Furthermore, we examine the deflection angle in the presence of a plasma medium and the effect of the plasma medium on the deflection angle. The deflection angle of the BH solution in the gauged super-gravity is computed using the Keeton-Petters approach. Utilizing the ray-tracing technique, we investigate the shadow of the corresponding BH and analyze the plots of the deflection angle and shadow to verify the influence of the plasma and algebraic thermodynamic parameters on the deflection angle and shadow.

Keywords: new Schwarzschild-like black hole, Gibbons-Werner and Keeton-Petters techniques, deflection angle, ray-tracing approach, shadow

DOI: 10.1088/1674-1137/ad2a60

I. INTRODUCTION

Black holes (BHs), as predicted by Einstein's theory of general relativity (GR), are significant objects that are thought to originate as a result of the gravitational collapse of enormous astronomical objects. Numerous experimental and observational studies support GR [1]. These investigations have revealed that experimental data, including those on gravity waves, wormholes, and gravitational lensing on BHs, are consistent with the theoretical predictions of this theory. Gravitational waves are ripples in the structure of the universe, which are created by the collision of enormous objects such as BHs. Gravitational waves are induced by the curvature of space-time. A distribution of matter between a source and an observer that can bend light from the source to the observer is known as the deflection angle (DA). The DA is useful in studying the universe's dark matter distribution and imaging the furthest galaxies. In GR, the expectation that light will bend as it approaches big objects is met. The DA phenomenon is highly useful for detecting BHs in the cosmos because it implies that light beams are bent owing to the curvature of spacetime. The DA is classified as a weak field in literature and helps determine the position of BH geometry.

Gibbon and Werner [2] adopted the Gauss-Bonnet theorem (GBT) to derive the DA of light beams. The integral in a finite domain defined by a light ray was calculated using this method. Werner then developed this formalism further by applying Nazim's method with the Randers-Finsler metric [3] to determine the DA by a Kerr-Newman BH. Recently, the DA in a static, spherical, symmetrical, and asymptotically flat region [4–7] was calculated using the finite distance between an observer and a light source. Moreover, the GBT has topological implications when applied to the geometries of wormholes and non-asymptotically flat spacetime [8, 9]. Jusufi and Övgün [10] recently made a significant contribution by discussing the quantum correction effects on light deflection caused by quantum-expanding Kerr BHs in a cosmic string. The DA in spacetimes with topological defects was calculated using both cosmic strings and global monopoles [11–14]. This strategy has been used in several studies for various spacetimes [15, 16].

Javed *et al*. [17] employed the light DA resulting from a Brane-Dicke wormhole in the weak field limit ap-

Received 11 January 2024; Accepted 19 February 2024; Published online 20 February 2024
* Supported by the National Natural Science Foundation of China (11975145)
† E-mail: riasatyasin@gmail.com
‡ E-mail: xiatc@shu.edu.cn
§ E-mail: awaiseducation@gmail.com
¶ E-mail: rimsha.babar10@gmail.com

proximation and examined the effect of the Brane-Dicke coupling parameter on weak gravitational lensing. Their findings offer a useful tool for immediately identifying the wormhole and naked singularity types and searching for evidence supporting the Brane-Dicke theory. They also used the GBT to determine the weak DA of light in the frame of an Einstein-Maxwell-Dilaton-axion BH [18] and investigated the effect of a plasma medium when light is deflected around a particular BH.

BHs are massive objects that are studied by GR at the center of our galaxy. It is commonly known that photons from a light source behind a BH cause the observer's sky in the dark area to appear as the "BH shadow." The BH shadow, which is an impose of the BH, provides essential information about the BH. To illustrate, from the BH shadow, one may extract the charge and spin of the BH [19–24] and limit certain additional parameters produced by changing gravities for the BH shadow [25–29]. Synge [30] and Luminet [31] investigated the shadow cast by an ideal circle, or BH, with spherical symmetry. They also provided formulas for the shadow's size and angular radius. Bardeen [32] was the first to investigate the shadow generated by a Kerr BH, and the dragging effect was found to distort the shape of the shadow. The BH shadow has been widely studied in literature. For instance, the BH shadow and photon sphere were investigated in dynamically shifting spacetimes in Ref. [33], and in Ref. [34], the implications of the cosmological constant on the BH shadow were examined. The shadow of a normal rotating BH was studied in Ref. [35], the shadow of a model-independent parameterized axisymmetric BH was computed in Ref. [36], and the quasinormal modes in the eikonal limit and the radius of the BH shadow were found to be related in [37, 38]. Additional important examinations of the BH shadow and DA were performed in [39–41]. The shadow cast by a dyon BH, also known as Kerr-Newman-Kasuya spacetime, was studied in [42], where it was concluded that the shadow image is affected by both its rotational momentum and dyon charge. Övgün *et al*. studied [43, 44] the DA for spacetime solutions, such as the generalized Einstein-Cartan-Kibble-Sciama and null aether theories, using the GBT and verified that weak deflection of BHs is effected in these theories. An extensive review of quasinormal modes, analytic greybody factors, and gravitational lensing in rotating BH spacetime, such as bumblebees, is presented in [45]. Using GR combined with the bumblebee theory, the investigation produced impressive results in four dimensions. This was demonstrated to be the more physically accurate metric form of a rotating bumblebee-like BH after presenting some of its physical characteristics. The light deflection in the spacetime of a rotating BH that is electrically charged was examined in [46] and considered in terms of its impact on the cosmological constant. The deflection for a Kerr-Newman anti-Sitter BH was also computed by exploiting the Rindler-Ishak technique extension.

A significant astrophysical BH is produced with BH mass and algebraic thermodynamic parameters. Furthermore, to obtain a thorough understanding of the features of a modified BH, the BH geometry under the impacts of the DA and BH shadow modifications must be analyzed. In addition, a BH is typically surrounded by plasma; therefore, the effects of plasma, BH mass, and algebraic thermodynamic parameters on the BH DA and shadow must also be investigated.

This paper is organized as follows. In Sec. II, we explore the DA of light for a new type of Schwarzschild BH in a non-plasma medium. In Section III, we investigate the DA for the new type of Schwarzschild BH in a plasma medium. In Sec. IV, we verify our results using the Keeton and Petter technique, Section V comprises the equation of motion for light rays under the influence of non-magnetized plasma to compute the shadow of the corresponding BH, and in Sec. VI, we discuss the results of our study.

II. DEFLECTION ANGLE IN A NON-PLASMA MEDIUM FOR A NEW TYPE OF SCHWARZSCHILD BLACK HOLE

The study of the DA in a non-plasma medium for a novel type of Schwarzschild BH forms the basis of this section. For this purpose, we consider the four-dimensional space-time metric of this new Schwarzschild BH, given as [47, 48]

$$\mathrm{d}s^2 = -G(r)\mathrm{d}t^2 + U(r)\mathrm{d}r^2 + r^2\mathrm{d}\Omega^2, \tag{1}$$

where $\mathrm{d}\Omega^2 = \mathrm{d}\theta^2 + \sin^2\theta\mathrm{d}\phi$ and $G(r) = \frac{1}{U(r)} = \left(1 - \frac{\mu}{r} + \frac{p^2}{r^2}\right)$. Moreover, the parameters M and p represent the BH mass and algebraic thermodynamic parameters, respectively. The parameter μ is associated with the BH mass defined by the relation $M = \frac{\mu}{2}$. By considering the metric function $G(r) = 0$, we can obtain the inner (r_-) and outer (r_+) horizons via

$$r_+ = \frac{1}{2}(\mu + \sqrt{\mu^2 - 4p^2}),\ r_- = \frac{1}{2}(\mu - \sqrt{\mu^2 - 4p^2}). \tag{2}$$

Figure 1 shows the behavior of the metric function $G(r_+)$. The left plot indicates this behavior for different choices of the algebraic parameter, whereas the right plot represents this behavior for different μ. In both plots, the metric function negatively increases and decreases, which indicates an unstable form.

The BH becomes an extreme BH at the condition

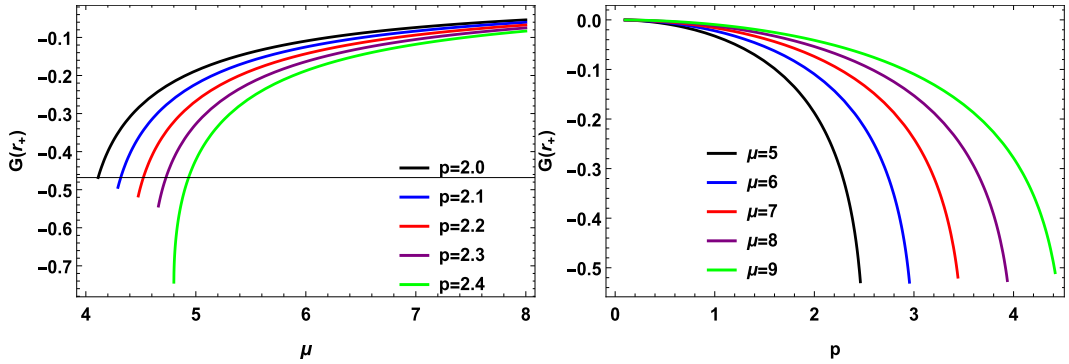

Fig. 1. (color online) Metric function $G(r_+)$ with respect to the ADM mass μ and algebraic parameter p.

$r_+ = r_-$. The relationship between the algebraic parameters and μ and the horizons is given as follows:

$$\mu = r_- + r_+, \quad p^2 = r_- r_+. \tag{3}$$

The condition $p^2 \leqslant \frac{\mu^2}{4}$ is always satisfied, except for the naked singularity at $r = 0$. Here, we investigate the BH bending angle in a non-plasma medium using the GBT. In the event that the tropical region is linked to the observer, source, and null photon, we can investigate $(\theta = \frac{\pi}{2})$. By setting $\mathrm{d}s^2 = 0$ in Eq. (1), we derive the optical metric via

$$\mathrm{d}t^2 = \frac{U}{G} dr^2 + \frac{r^2}{G}\mathrm{d}\phi. \tag{4}$$

The following formula yields the non-zero Christoffel symbols for the given metric:

$$\begin{aligned}
\Gamma^1_{11} &= \frac{U'(r)}{2U(r)} - \frac{G'(r)}{2G(r)}, \\
\Gamma^2_{12} &= \frac{G(r)}{r} - \frac{G'(r)}{2}, \\
\Gamma^1_{22} &= \frac{r^2 G'(r)}{2U(r)G(r)} - \frac{r}{U(r)},
\end{aligned} \tag{5}$$

where 1 and 2 indicate the r and ϕ coordinates, respectively, and the Ricci scalar for the given metric is computed as follows:

$$R = \frac{2G''(r)U(r)G(r) - G'(r)U'(r)G(r) - G'^2(r)U(r)}{2U^2(r)G^2(r)}. \tag{6}$$

To calculate the Gaussian curvature, we use the formula

$$\mathbb{K} = \frac{R}{2}. \tag{7}$$

Inserting Eq. (6) into Eq. (7), the Gaussian curvature can be computed via

$$\mathbb{K} \approx \frac{\mu}{r^3} - \frac{3\mu^2}{4r^4} - \frac{3p^2}{r^4} + \frac{3\mu p^2}{r^5} + \frac{2p^4}{r^6}. \tag{8}$$

This formula is helpful in calculating the DA for a new type of Schwarzschild BH solution utilizing the GBT in the region of the non-singular domain M_e :

$$\int\int_{M_e} \mathbb{K}\mathrm{d}S + \oint_{\partial M} k\mathrm{d}t + \sum_i \epsilon_i = 2\pi\chi(\mathbb{K}). \tag{9}$$

In the above expression, $k = \bar{g}(\nabla_{\dot{\zeta}}\dot{\zeta}, \ddot{\zeta})$ denotes the geodesic curvature. The unit acceleration vector $\ddot{\zeta}$ is denoted by $\bar{g}(\ddot{\zeta}, \dot{\zeta}) = 1$, whereas the exterior angle of the *ith* vertex is expressed as $\epsilon_i i$. The associated jump angles decrease to $\frac{\pi}{2}$ as $e \to \infty$, yielding $\theta_O + \theta_s \to \pi$, and $\zeta(\mathbb{K}) = 1$ is the Euler characteristic. Therefore, the above equation can be rewritten as

$$\int\int_{M_e} \mathbb{K}\mathrm{d}S + \oint_{\partial M_e} k\mathrm{d}t + \epsilon_i = 2\pi\zeta(S_e). \tag{10}$$

To obtain the geodesic curvature, we use the following relation:

$$k(W_e) = |\nabla_{\dot{W}_e}\dot{W}_e|. \tag{11}$$

The radial component of geodesic curvature can be defined as

$$(\nabla_{\dot{W}_e}\dot{W}_e)^r = \dot{W}_e^{\phi}\partial_{\phi}\dot{W}_e^r + \Gamma^1_{22}(\dot{W}_e^{\phi})^2. \tag{12}$$

Therefore, following result can be computed for a large value of e, such that $W_e := r(\phi) = e = \text{constant}$ as

$$(\nabla_{\dot{W}_e}\dot{W}_e)^r \to \frac{1}{e}. \tag{13}$$

Because there is no topological flaw in the geodesic curvature, $k(W_e) \to e^{-1}$. Nevertheless, it can be stated as $\mathrm{d}t = e\mathrm{d}\phi$ by applying the optical metric Eq. (4). Consequently, we have

$$k(W_e)\mathrm{d}t = \mathrm{d}\phi. \tag{14}$$

Now, the following equation may be obtained by utilizing the previous expression:

$$\int\int_{M_e} \mathbb{K}\mathrm{d}S + \oint_{\partial M_e} k\mathrm{d}t \xrightarrow{h\to\infty} \int\int_{T\infty} \mathbb{K}\mathrm{d}S + \int_0^{\pi+\psi} \mathrm{d}\phi. \tag{15}$$

In the weak field limitations, the $0th$ order light ray is computed as $r(t) = \dfrac{b}{\sin\phi}$. Equations (9) and (15) can be used to obtain the bending angle as

$$\psi \approx -\int_0^{\pi}\int_{\frac{b}{\sin\phi}}^{\infty} \mathbb{K}\sqrt{\det\vec{g}}\mathrm{d}r\mathrm{d}\phi, \tag{16}$$

where $\sqrt{\det\vec{g}}$ is computed as

$$\sqrt{\det\vec{g}} = r\left(1 - \frac{\mu}{r} + \frac{p^2}{r^2}\right)^{\frac{-3}{2}}. \tag{17}$$

The DA is computed using the Gaussian curvature up to the leading order terms:

$$\psi \approx \frac{2\mu}{b} - \frac{3p^2\pi}{4b^2} - \frac{3\mu^2\pi}{16b^2} + \frac{4\mu p^2}{3b^3} + O(p^4). \tag{18}$$

The above DA depends on the impact parameter b, algebraic parameter p, and ADM mass μ. We can also observe that the impact parameter has an inverse relationship with the DA. It is important to note that our results are similar to the Reissner–Nordström BH given in [49, 50] without higher order magnetic correction terms. Moreover, by setting $\mu = 2M$ and $p = 0$, that is, an improved relationship for the trajectory of a light ray in the integration domain, our expected first-order DAs are reduced to the standard Schwarzschild BH DA, $\psi_{Sch} = \dfrac{4M}{b}$, found in [51].

Figure 2 indicates the behavior of the DA ψ with the impact parameter b for different choices of μ and p. From both plots, we graphically observe that the impact parameter has an inverse relationship with the DA. The DA decreases as the impact parameter increases in the region $1 \leqslant b \leqslant 10$. Moreover, the ADM mass has a direct relationship with the angle, whereas the algebraic parameter has an inverse relationship. We can also conclude that the light bends with a maximum angle for small values of the impact parameter.

III. DEFLECTION ANGLE IN A PLASMA MEDIUM FOR A NEW TYPE OF SCHWARZSCHILD BLACK HOLE

Next, the DA in a plasma medium is calculated. Let v be the speed of light through hot ionized gas, representing the effects of plasma. The refractive index, $n(r) = c/v$, for the given BH is defined as [52]

$$n = \sqrt{1 - \frac{\omega_e^2}{\omega_\infty^2}\frac{U}{G}}, \tag{19}$$

where ω_e^2 represents electron plasma frequency, and ω_∞^2 represents the photon frequency determined at infinity by the observer. The associated optical metric is defined as

$$\mathrm{d}\sigma^2 = g_{ij}^{\mathrm{opt}}\mathrm{d}x^i\mathrm{d}x^j = n^2\left(\frac{U}{G}\mathrm{d}r^2 + \frac{r^2}{G}\mathrm{d}\phi\right). \tag{20}$$

The optical Gaussian curvature for the new type of

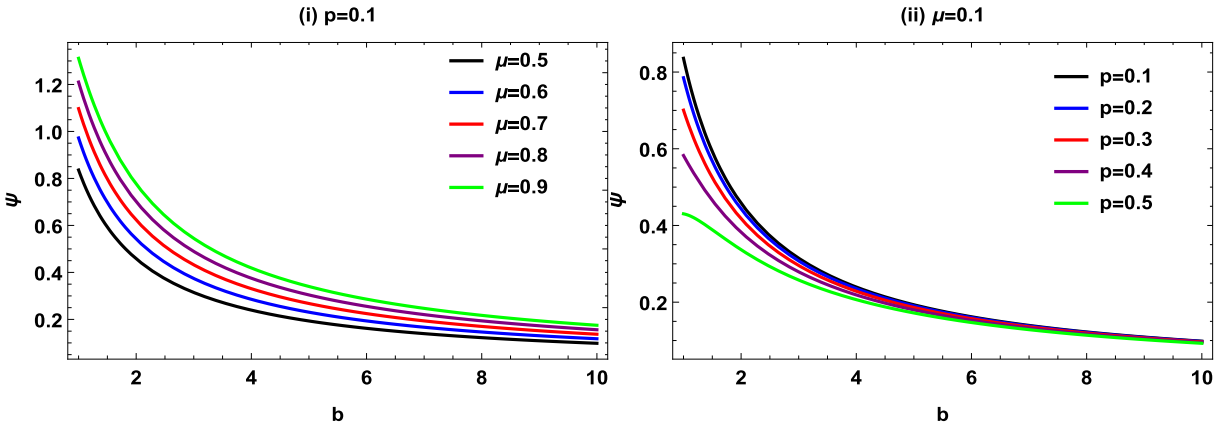

Fig. 2. (color online) Deflection angle ψ with respect to the impact parameter b. The left plot shows the behavior for various μ with fixed $p = 0.1$, and the right plot shows the behavior for different p with fixed $\mu = 0.1$.

Schwarzschild BH can be calculated as

$$K \simeq \frac{\mu}{r^3} - \frac{3\mu^2}{4r^4} - \frac{3p^2}{r^4} + \frac{3\mu p^2}{r^5} + \frac{3\mu\omega_e^2}{2r^3\omega_\infty^2} - \frac{3\mu^2\omega_e^2}{r^4\omega_\infty^2} - \frac{5p^2\omega_e^2}{r^4\omega_\infty^2} + \frac{13\mu p^2\omega_e^2}{r^5\omega_\infty^2}. \tag{21}$$

We calculate the bending angle using the GBT. To achieve this, we use the approximation $r(t) = \frac{b}{\sin\phi}$ at the $0th$ order, and the DA is obtained as

$$\psi_1 \approx -\lim_{R\to 0}\int_0^{\pi}\int_{b/\sin\phi}^{\infty} \mathbb{K}\sqrt{\det\vec{g}}\,\mathrm{d}r\mathrm{d}\phi. \tag{22}$$

For the leading order terms of the new form of Schwarzschild BH under the impacts of a plasma medium and using the values of Gaussian curvature obtained by inserting Eq. (21) into Eq. (22), the DA is computed as

$$\psi_1 \approx \frac{2\mu}{b} - \frac{3p^2\pi}{4b^2} - \frac{3\mu^2\pi}{16b^2} + \frac{4\mu p^2}{3b^3} + \frac{2\mu\omega_e^2}{\omega_\infty^2 b} - \frac{3p^2\pi\omega_e^2}{4b^2\omega_\infty^2} - \frac{3\mu^2\pi\omega_e^2}{16b^2\omega_\infty^2} + \frac{4\mu p^2\omega_e^2}{3b^3\omega_\infty^2} + O(p^4). \tag{23}$$

The above expression for the DA in a plasma medium is dependent on the impact parameter b, ADM mass μ, algebraic parameter p, and electron and photon frequencies ω_e and ω_∞, respectively. It is important to note that when $\frac{\omega_e}{\omega_\infty} \to 0$, the above equation reduces to Eq. (18).

Figure 3 represents the graphical behavior of the DA ψ with b for different choices of μ and p. From both plots, we note that the impact parameter also has a inverse relationship with the angle in the presence of a plasma medium. The DA decreases when the impact parameter increases in the region $1 \leqslant b \leqslant 15$. Moreover, the algebraic parameter has an inverse relationship with the angle, whereas the ADM mass has a direct relationship with the angle in the presence of plasma. We observe a strong deflection at small values of the impact parameter.

IV. DEFLECTION ANGLE ANALYSIS USING THE KEETON AND PETTERS METHOD

The DA of the novel Schwarzschild BH solution is determined using the Keeton and Petters approach. Keeton and Petters modified the original approach to make it more in line with their methodology and obtain outcomes [53, 54]. Post-post Newtonian (PPN) theory provides a straightforward method for handling any gravity theories, where the weak deflection limit is expressed as a single variable m series expansion. For this purpose, we can take space-time in the form

$$\mathrm{d}s^2 = Y\mathrm{d}t^2 + Z\mathrm{d}r^2 + r^2\mathrm{d}\Omega^2. \tag{24}$$

The metric functions Y and Z can be written in a PPN series as

$$Y = 1 + 2l_1\left(\frac{\gamma}{n^2}\right) + 2l_2\left(\frac{\gamma}{n^2}\right)^2 + 2l_3\left(\frac{\gamma}{n^2}\right)^3 + ...,$$

$$Z = 1 - 2s_1\left(\frac{\gamma}{n^2}\right) + 4s_2\left(\frac{\gamma}{n^2}\right)^2 - 8s_3\left(\frac{\gamma}{n^2}\right)^3 + ..., \tag{25}$$

where γ represents the Newtonian potential in three-dimensions and can be defined as

$$\frac{\gamma}{n^2} = -\frac{m}{r}. \tag{26}$$

The DA ψ_2 is expressed in a series expansion form as follows:

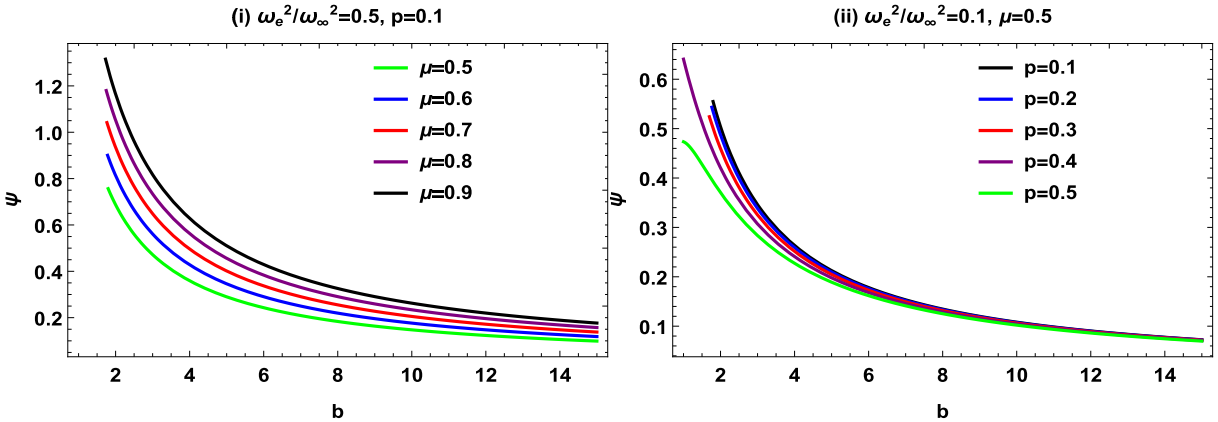

Fig. 3. (color online) Deflection angle ψ with respect to the impact parameter b. The left plot shows the behavior for various μ, and the right plot shows the behavior for different p.

$$\psi_2 \approx J_1\left(\frac{m}{b}\right)+J_2\left(\frac{m}{b}\right)^2+J_3\left(\frac{m}{b}\right)^3+O\left(\frac{m}{b}\right)^4. \tag{27}$$

Here,

$$J_1=2(l_1+s_1), \qquad J_2=(2l_1^2-l_2+l_1s_1+\frac{s_1^2}{4}+s_2)\pi, \tag{28}$$

$$J_3=\frac{2}{3}\left(35l_1^3+15l_1^2l_1+3l_1(10l_2+s_1^2-4s_1^2 +6l_3+s_1^3-6l_2s_1-4s_1s_2+s_3\right). \tag{29}$$

Now, we compare Y with $G(r)$ and Z with $U(r)$ given in Eq. (1) and compute the PPN coefficients as follows:

$$l_1=\frac{\mu}{2m}, \quad l_2=-\frac{p^2}{2m^2}, \quad l_3=0, \quad s_1=\frac{\mu}{2m}, \quad s_2=-\frac{(\mu^2-p^2)}{4m^2}, \quad s_3=-\frac{\mu^3-2p^2\mu}{8m^3}. \tag{30}$$

After inserting all of the above co-efficients into Eqs. (28) and (29), we obtain

$$J_1=\frac{2\mu}{m}, \quad J_2=-\frac{17\mu^2\pi}{16m^2}-\frac{3p^2\pi}{4m^2}, \quad J_3=\frac{9p^2\mu}{2m^3}. \tag{31}$$

After substituting the values from Eq. (27) into Eq. (31), we obtain the DA as

$$\psi_2 \approx \frac{2\mu}{m}\left(\frac{m}{b}\right)-\left(\frac{17\mu^2\pi}{16m^2}+\frac{3p^2\pi}{4m^2}\right)\left(\frac{m}{b}\right)^2 -\left(\frac{9p^2\mu}{2m^3}\right)\left(\frac{m}{b}\right)^3+O\left(\frac{m}{b}\right)^4. \tag{32}$$

The values of m, p, b, and μ have an impact on the required DA.

V. STUDY OF LIGHT RAYS IN A NON MAGNETIZED PLASMA

To obtain the conditions of null geodesics, we can derive the equations of motion and consider the impact of an electron plasma frequency $\omega_e(r)$ on a non-magnetized cold plasma through the Hamiltonian [55] of the moving photon to study the shadow of the new type of Schwarzschild BH:

$$H=\frac{1}{2}\left(g^{ik}j_ij_k+\omega_p(r^2)\right)=\frac{1}{2}\left(-\frac{f_t^2}{G(r)}+\frac{f_r^2}{U(r)}+f_\phi^2+\omega_e(r^2)\right). \tag{33}$$

The Hamiltonian in Eq. (33) for a two-fluid source is derived from Maxwell's equations, and the quantities of continuous motion f_t and f_ϕ connected to the energy $-f_t=E$ and angular momentum $f_\phi=L$ can be defined to obtain the equations of motion for photons:

$$\dot{f}_i=-\frac{\partial H}{\partial x^i}, \quad \dot{x^i}=-\frac{\partial H}{\partial f_i}, \tag{34}$$

which imply that

$$\dot{f}_t=-\frac{\partial H}{\partial t}=0, \tag{35}$$

$$\dot{f}_\psi=-\frac{\partial H}{\partial \psi}=0, \tag{36}$$

$$\dot{f}_r=-\frac{\partial H}{\partial r}=0, \tag{37}$$

where f_r gives the radial momentum and can be defined as

$$\dot{f}_r=-\frac{\partial H}{\partial r}=\frac{1}{2}\left(-\frac{f_t^2G'(r)}{G(r)^2}+\frac{f_r^2U'(r)}{U(r)^2}+\frac{d}{dr}f_\psi^2-\frac{d}{dr}\omega_e(r^2)\right). \tag{38}$$

Moreover,

$$\dot{t}=\frac{\partial H}{\partial f_t}=-\frac{f_t}{G(r)}, \tag{39}$$

$$\dot{\phi}=\frac{\partial H}{\partial f_\phi}=-f_\phi, \tag{40}$$

$$\dot{r}=\frac{\partial H}{\partial f_r}=-\frac{f_r}{U(r)}, \tag{41}$$

with $H=0$, such that

$$0=-\frac{f_t^2}{G(r)}+\frac{f_r^2}{U(r)}+f_\phi^2+\omega_e(r^2), \tag{42}$$

In this case, the prime denotes differentiation with respect to r, whereas the dot denotes differentiation with respect to an affine parameter λ.

It is evident from Eqs. (35) and (36) that f_t and f_ϕ are motion constants. The formula converts the frequency ω observed by a static observer into a function of r as follows:

$$\omega(r)=\frac{\omega_0}{\sqrt{G(r)}}. \tag{43}$$

We use Eqs. (40) and (41) to obtain the orbit equation

$$\frac{\mathrm{d}r}{\mathrm{d}\psi}=\frac{\dot{r}}{\dot{\phi}}=\frac{f_r}{U(r)f_\phi}. \tag{44}$$

After substituting for f_r in Eq. (43),

$$\frac{\mathrm{d}r}{\mathrm{d}\phi}=\pm\frac{1}{\sqrt{U(r)}}\sqrt{\frac{p(r)^2}{f_\psi^2}-1}, \tag{45}$$

where ω_0 denotes the frequency measured by a static observer, and we define the function

$$p(r)^2=\frac{1}{G(r)}\left(1-G(r)\frac{\omega_e^2}{\omega_0^2}\right). \tag{46}$$

Given that X denotes the turning point of the trajectory, $\frac{\mathrm{d}r}{\mathrm{d}\phi|_X}=0$ must hold. This formula connects X to the constant of motion $\frac{f_\phi}{\omega_0}$ as

$$p(X)^2=\frac{f_\phi^2}{\omega_0^2}. \tag{47}$$

It is anticipated that a stationary observer at point r_0 will release light beams into the past with an angular radius β [55] relative to the radial direction:

$$\cot\beta=\pm\frac{\sqrt{g_{rr}}}{\sqrt{g_{\phi\psi}}}\frac{\mathrm{d}r}{\mathrm{d}\phi}\Big|_{r=r_0}=\pm\frac{1}{\sqrt{U(r)}}\frac{\mathrm{d}r}{\mathrm{d}\phi}\Big|_{r=r_0}. \tag{48}$$

Equation (45) can be used to rewrite the orbit equation (Eq. (47)) in the event that the light beam disappears after reaching a minimal radius R:

$$\frac{\mathrm{d}r}{\mathrm{d}\phi}=\pm\frac{\sqrt{1}}{\sqrt{U(r)}}\sqrt{\frac{p(r)^2}{p(R)^2}-1}. \tag{49}$$

For the angle β, we obtain

$$\cot^2\beta=\frac{p(r)^2}{p(X)^2}-1. \tag{50}$$

By utilizing the identity, we have

$$1+\cot^2\beta=\frac{1}{\sin^2\beta} \tag{51}$$

Inserting Eq. (51) into Eq. (50), we obtain

$$\sin^2\beta=\frac{p(r)^2}{p(R)^2}. \tag{52}$$

Light rays traveling asymptotically toward a circular light orbit at radius r_{ph} define the boundary of the shadow β. For this reason, $R\to r_{ph}$ in Eq. (52) yields the angular radius of the shadow as follows:

$$\sin^2\beta=\frac{p(r_{ph})^2}{p(r_0)^2}, \tag{53}$$

where $p(r)$ is obtained using Eq. (46). In numerous instances, it is possible to presume that the observer is located in an area with a negligibly small plasma density. Therefore, Eq. (46) gives

$$p(r)^2=\frac{1}{G(r_0)}, \tag{54}$$

and Eq. (54) implies that

$$\sin^2\beta=\frac{G(r_0)}{G(r_{ph})}\left(1-\frac{G(r_{ph})\omega_e(r_{ph}^2)}{\omega_o^2}\right). \tag{55}$$

After substituting all values, we obtain

$$\begin{aligned}\sin^2\beta=&\left(\frac{\omega_o^2}{p^2r_0r_{ph}\mu}\right)\left(r_{ph}^2+\frac{\omega_e^2}{\omega_o^2}\left(p^2+r_{ph}^2\mu+r_{ph}^2\right)\right)\\&\left(p^4\mu-p^4r_{ph}+p^2r_{ph}^2\mu-r_0\mu\left(p^2\mu-p^2r_{ph}+r_{ph}^2\mu\right)\right.\\&\left.+r_0^2\left(p^2\mu-p^2r_{ph}+r_{ph}^2\mu\right)\right).\end{aligned} \tag{56}$$

The shadow β depends on the algebraic parameter p, ADM mass μ, plasma frequencies ω_0 & ω_e, photon radius r_{ph}, and observer radius r_0.

Figure 4 illustrates the variations in the shadow β in terms of the photon r_{ph} and observer r_0 radii. In plot (i), the shadow exponentially increases with variations in r_0 with fixed $p=0.1$, $\mu=10$, $\omega_e=0.2$, and $\omega_0=0.3$ in the region $0\leqslant r_{ph}\leqslant 2.5$. The shadow is noticeably smaller for larger values of r_0. This inverse proportionality between the shadow and photon radius can account for the reduction in the shadow β as r_0 increases.

Plot (ii) illustrates the behavior of the shadow β in terms of the observer radius r_0 with variations in r_{ph} with fixed $p=5$, $\mu=10$, $\omega_e=0.2$, and $\omega_0=0.3$ in the region $3\leqslant r_0\leqslant 7$. Symmetry can be observed in the shadow, along with a sharp edge at $\beta=0$.

The contour plots of the new type of Schwarzschild BH shadow can be plotted in the form of the celestial coordinates α and β.

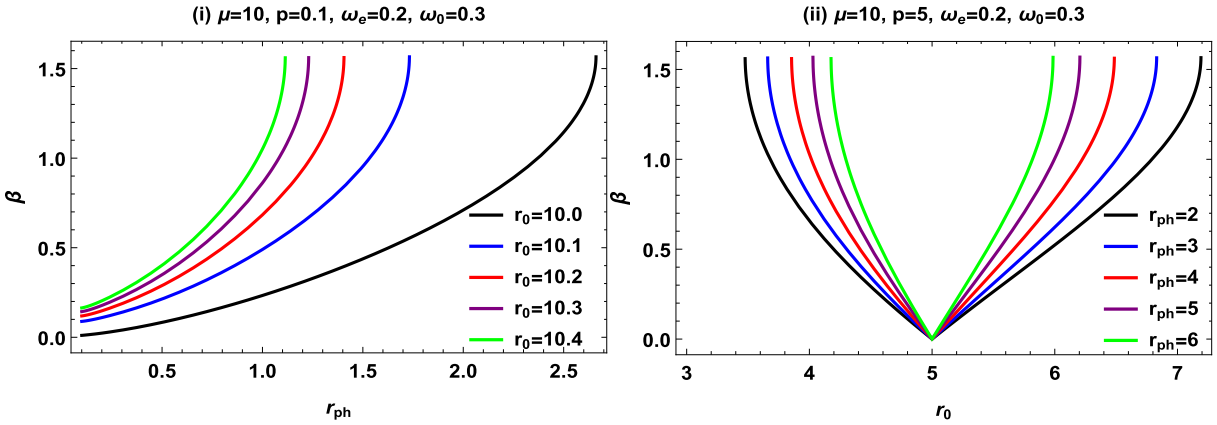

Fig. 4. (color online) Shadow in terms of the radii r_{ph} and r_0. The left plot shows the behavior for various r_0 , and the right plot shows the behavior for different r_{ph}.

Figure 5 (i) shows the contour plots of the shadow for different choices of photon radius, that is, $r_{ph}=1$ (purple), 2 (yellow), 3 (green), 4 (orange), 5 (blue), and 6 (red). The size of shadow radius increases with increasing photon radius.

Figure 5 (ii) shows the contour plots of the shadow with variations in radius $r_0=5$(purple), 5.5 (yellow), 6 (green), 6.5 (orange), 7 (blue), and 7.5 (red). The shadow radius increases with increasing observer radiusr_0 and is larger than the photon radius. Figure 6 (i) depicts the contour plots of the shadow for different choices of ADM mass $\mu=1$(purple), 1.5 (yellow), 2 (green), 2.5 (orange), 3 (blue), and 3.5 (red). The inverse relationship between the shadow radius and ADM mass μ suggests that the radius decreases with increasing mass influence.

Figure 6 (ii) represents the contour plots of the shadow with variations in the algebraic parameter $p=0.1$ (purple), 0.5 (yellow), 1 (green), 1.5 (orange), 2 (blue), and 2.5 (red). The size of shadow radius increases with increasing p.

VI. CONCLUSION

This study uses mathematical calculations to analyze the weak DA and shadow of a novel type of Schwarzschild BH in the background of a non-plasma/plasma framework. The weak DA of this BH is then obtained using the GBT and Gibbons and Werner method to investigate the gravitational field of the BH and its fundamental properties, including the mass and algebraic parameters, the type of light bending, and the underlying validity of Einstein's theory. These help us understand the dynam-

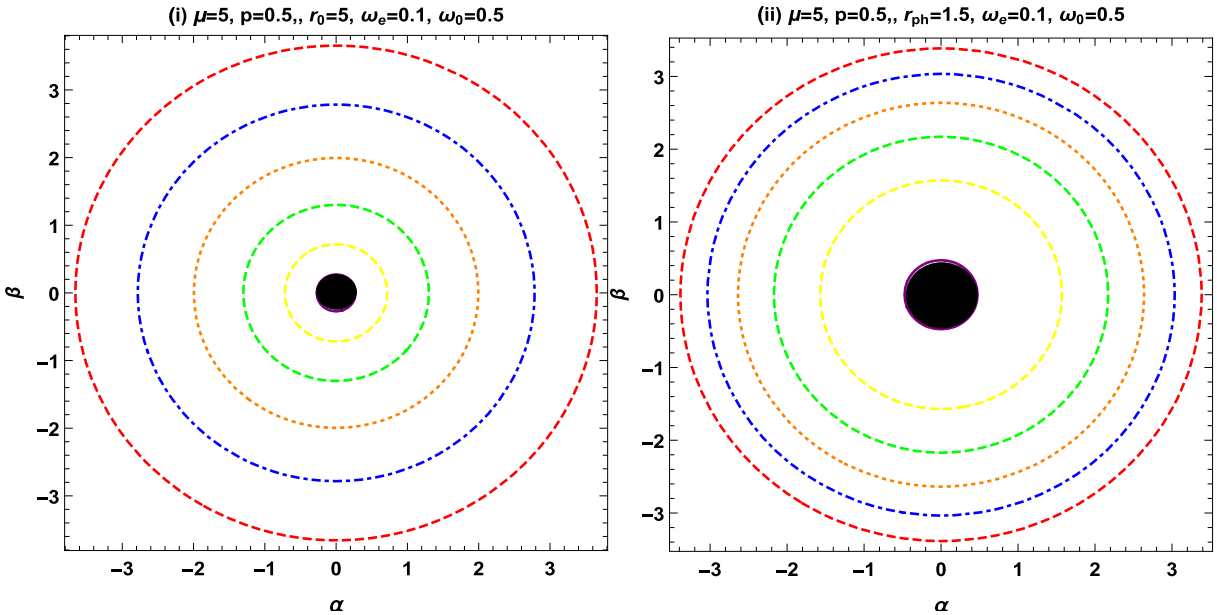

Fig. 5. (color online) Shadow of the new type of Schwarzschild BH for different choices of radius r_{ph} and r_0 and fixed values of $\mu=5, p=0.5, \omega_e=0.1$, and $\omega_0=0.5$.

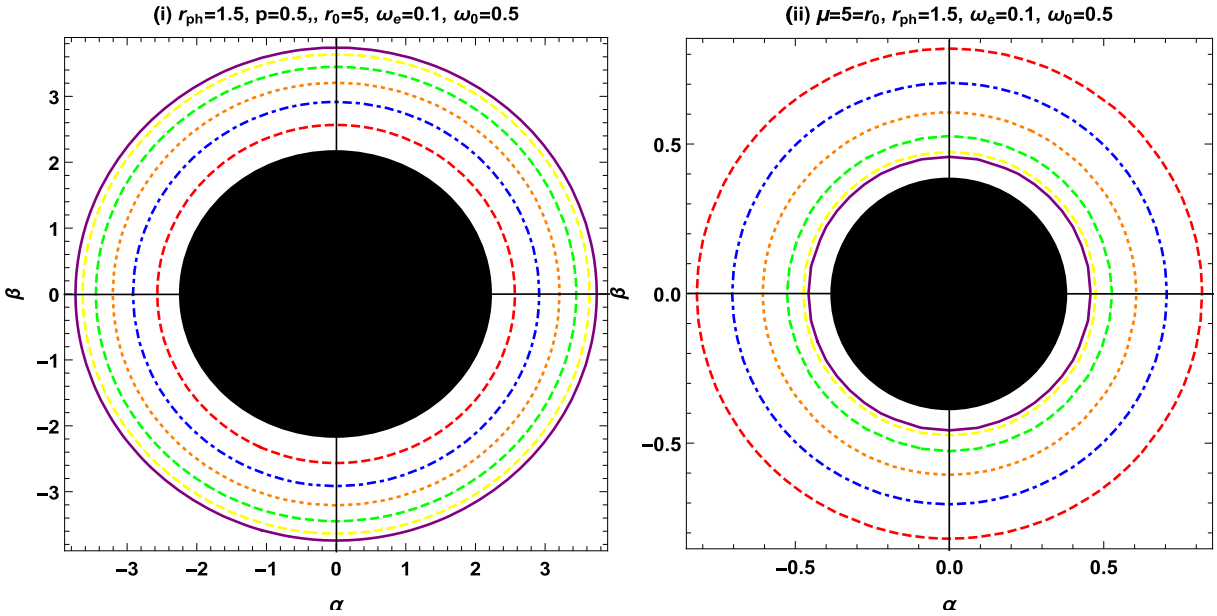

Fig. 6. (color online) Shadow of the new type of Schwarzschild BH for different choices of the ADM mass μ and algebraic parameter p and fixed values of $r_0 = 5$, $r_{ph} = 1.5$, $\omega_e = 0.1$, and $\omega_0 = 0.5$.

ics of BHs and guide observational astronomers in terms of what and what not to expect. The DA for the new type of Schwarzschild BH is found to vary greatly, with an increase caused by its regulating parameters.

First, we investigate the new type of Schwarzschild BH solution in a non-plasma frame and determine that the DA depends on the impact parameter b, ADM mass μ, and algebraic parameter p. It is worth noting that our result in Eq. (18) is similar to the Reissner–Nordström BH result given in [49, 50], without higher order magnetic correction terms. Moreover, by setting $\mu = 2M$ and $p = 0$ in Eq. (18), our result for the DA is reduced to the DA of the standard Schwarzschild BH, $\psi_{Sch} = \dfrac{4M}{b}$.

We also graphically conclude that the impact parameter has an inverse relationship with the DA. Moreover, the ADM mass has a direct relationship with the angle, whereas the algebraic parameter has an inverse relationship. We also conclude that for small values of the impact parameter, the light bends with a maximum angle.

Furthermore, we investigate the DA in a plasma frame and find that it is dependent on the impact parameter b, ADM mass μ, algebraic parameter p, and plasma frequencies ω_∞ and ω_e. We also conclude that when $\dfrac{\omega_e}{\omega_\infty} \to 0$, the results of the DA in a plasma medium (Eq. (23)) reduce to the results in a non-plasma medium (Eq. (18)). From our graphical analysis in the plasma medium, the ADM mass has an inverse relationship with the angle, whereas the algebraic parameter has a direct relationship with the angle. We observe a strong deflection in the plasma frame compared to the non-plasma medium.

Additionally, we apply the Keeton and Petters method to calculate and verify the results of the DA. We examine the dependence of the DA of the Keeton and Petters technique on the impact parameter, algebraic parameter, and ADM mass.

Finally, we study the shadow of the new type of Schwarzschild BH using an equation of motion for light rays under the impact of non-magnetized plasma. The magnitude of the shadow is dependent on a variety of parameters. The shadow β depends on the algebraic parameter p, ADM mass μ, plasma frequencies ω_0 & ω_e, photon radius r_{ph}, and observer radius r_0. We also plot contour graphs for the shadow of the new type of Schwarzschild BH and analyze the effects of the photon and observer radii, algebraic parameter, and ADM mass on the BH shadow. We conclude that the size of the shadow increases with increasing algebraic parameter and photon and observer radii. Moreover, we observe the inverse relationship between the shadow radius and ADM mass μ, suggesting that the radius decreases with increasing mass influence.

CONFLICT OF INTEREST

The authors declare no conflicts of interest.

DATA AVAILABILITY STATEMENT

The data that support the findings of this study are available from the corresponding author upon reasonable request.

References

[1] A. Einstein, Annalen Phys. **49**, 769 (1916)
[2] G. W. Gibbons and M. C. Werner, Class. Quant. Grav. **25**, 235009 (2008)
[3] M. C. Werner, Gen. Rel. Grav. **44**, 3047 (2012)
[4] A. Ishihara, Y. Suzuki, T. Ono *et al.*, Phys. Rev. D **94**, 084015 (2016)
[5] H. Arakida, Gen. Rel. Grav. **50**, 48 (2018)
[6] T. Ono, A. Ishihara, and H. Asada, Phys. Rev. D **98**, 044047 (2018)
[7] T. Ono, A. Ishihara and H. Asada, Phys. Rev. D **96**, 104037 (2017)
[8] K. Jusufi, A. Övgün, and A. Banerjee, Phys. Rev. D **96**, 084036 (2017)
[9] K. Jusufi and A. Övgün, Phys. Rev. D **97**, 024042 (2018)
[10] K. Jusufi and A. Övgün, Int. J. Geom. Meth. Mod. Phys. **16**, 1950116 (2019)
[11] K. Jusufi, M. C. Werner, A. Banerjee *et al.*, Phys. Rev. D **95**, 104012 (2017)
[12] K. Jusufi, I. Sakalli, and A. Övgün, Phys. Rev. D **96**, 024040 (2017)
[13] T. Ono, A. Ishihara, and H. Asada, Phys. Rev. D **99**, 124030 (2019)
[14] A. Övgün, Phys. Rev. D **99**, 104075 (2019)
[15] A. Övgün, Phys. Rev. D **98**, 044033 (2018)
[16] W. Javed, J. Abbas, and A. Övgün, Eur. Phys. J. C **79**, 694 (2019)
[17] W. Javed, R. Babar, and A. Övgün, Phys. Rev. D **99**, 084012 (2019)
[18] W. Javed, R. Babar, and A. Övgün, Theory. Phys. Rev. D **100**, 104032 (2019)
[19] R. Takahashi, Astrophys. J. **611**, 996 (2004)
[20] N. Tsukamoto, Z. Li, and C. Bambi, JCAP **1406**, 043 (2014)
[21] A. F. Zakharov, A. A. Nucita, F. D. Paolis *et al.*, New Astron. **10**, 479 (2005)
[22] K. Hioki and K. Maeda, Phys. Rev. D **80**, 024042 (2009)
[23] A. F. Zakharov, Phys. Rev. D **90**, 062007 (2014)
[24] Z. Li and C. Bambi, JCAP **1401**, 041 (2014)
[25] J. C. S. Neves, Eur. Phys. J. C **80**, 717 (2020)
[26] L. Amarilla, E. F. Eiroa, and G. Giribet, Phys. Rev. D **81**, 124045 (2010)
[27] J. W. Moffat, Eur. Phys. J. C **75**, 130 (2015)
[28] L. Amarilla and E. F. Eiroa, Phys. Rev. D **85**, 064019 (2012)
[29] L. Amarilla and E. F. Eiroa, Phys. Rev. D **87**, 044057 (2013)
[30] J. L. Synge, Mon. Not. Roy. Astron. Soc. **131**, 463 (1966)
[31] J. P. Luminet, Astron. Astrophys. **75**, 228 (1979)
[32] J. M. Bardeen, *Timelike and Null Geodesics of the Kerr Metric* (Gordon and Breach: New York, NY, USA, 1973)
[33] A. K. Mishra, S. Chakraborty, and S. Sarkar, Phys. Rev. D **99**, 104080 (2019)
[34] V. Perlick, O. Y. Tsupko and G. S. Bisnovatyi-Kogan, Phys. Rev. D **97**, 104062 (2018)
[35] A. Abdujabbarov, M. Amir, B. Ahmedov *et al.*, Phys. Rev. D **93**, 104004 (2016)
[36] Z. Younsi, A. Zhidenko, L. Rezzolla *et al.*, Phys. Rev. D **94**, 084025 (2016)
[37] K. Jusufi, Phys. Rev. D **101**, 124063 (2020)
[38] R. A. Konoplya, Phys. Lett. B **804**, 135363 (2020)
[39] X. He, T. Xu, Y. Yu *et al.*, Ann. Phys. **451**, 169247 (2023)
[40] X. He, S. Zhu, Y. Yu *et al.*, Int. J. Geom. Methods Mod. Phys. **20**, 2350205 (2023)
[41] R. Ali, M. Awais, and A. Mahmood, Annalen der Physik **535**, 2300236 (2023)
[42] A. Övgün, I. Sakalli, and J. Saavedra, JCAP **10**, 041 (2018)
[43] A. Övgün and I. Sakalli, Class. Quantum Grav. **37**, 225003 (2020)
[44] A. Övgün, I. Sakalli, and J. Saavedra, Chinese Phys. C **44**, 125105 (2020)
[45] M. Mangut, H. Gürsel, S. Kanzi *et al.*, Universe **9**(5), 225 (2023)
[46] M. Mangut, H. Gürsel and I. Sakalli, Astroparticle Physics **144**, 102763 (2023)
[47] W. X. Chen and Y. G. Zheng, arXiv: 2204.05470
[48] Z. Akhtar, R. Babar, and R. Ali, Ann. Phys. **448**, 169190 (2023)
[49] Y. Kumaran and Ali Övgön, Symmetry **14**, 2054 (2022)
[50] M. H. Seçuka and Ö. Delice, Eur. Phys. J. Plus **135**, 610 (2020)
[51] W. Javed, J. Abbas, and A. A. Övgün, Ann. Phys. **418**, 168183 (2020)
[52] G. Crisnejo and E. Gallo, A unified treatment. Phys. Rev. D **97**, 124016 (2018)
[53] C. R. Keeton and A. Petters, Phys. Rev. D **72**, 104006 (2005)
[54] C. R. Keeton and A. Petters, Phys. Rev. D **73**, 044024 (2006)
[55] I. Cimdikera, D. Demirb, and A. Övgün, Phys. Dark Universe **34**, 100900 (2021)